Article type : Method Article

METHOD ARTICLE

Method for Visible Light Induced Photocatalytic Degradation of Methylparaben in Water Using Nanostructured Ag/AgBr@m-WO_3

M. A. Suliman[a], M. A. Gondal[b*], M. A. Dastageer[b], Gaik-Khuan Chuah[c],
C. Basheer[a]

[a]*Department of Chemistry, King Fahd University of Petroleum and Minerals, P.O Box 5047, Dhahran 31261, Saudi Arabia*

[b]*Laser Research Group, Department of Physics, King Fahd University of Petroleum and Minerals, P.O Box 5047, Dhahran 31261, Saudi Arabia*

[c]*Department of Chemistry, National University of Singapore, Science Drive 2, Kent Ridge, Singapore 117543*

Corresponding author's email: magondal@kfupm.edu.sa (Mohammed Gondal)

Abstract

An efficient method of photocatalytic degradation of methylparaben in water using Ag nanoparticles (NPs) loaded AgBr-mesoporous-WO_3 composite photocatalyst (Ag/AgBr@m-WO_3), under visible light is presented. In this process, quantification of methylparaben in water was carried out by high-performance liquid chromatography (HPLC) and the HPLC results showed a significant reduction of methylparaben in water due to the enhanced of photo-catalytic degradation efficiency of Ag/AgBr@m-WO_3. For the material synthesis, highly ordered mesoporous-WO_3 (m-WO_3) was initially synthesized by sol-gel method and AgBr nanoparticles (NPs) were subsequently introduced in the pores of m-WO_3, and finally, the Ag nanoparticles were introduced by light irradiation. The enhanced photocatalytic degradation of methylparaben in water is attributed to the formation of surface plasmonic

This article has been accepted for publication and undergone full peer review but has not been through the copyediting, typesetting, pagination and proofreading process, which may lead to differences between this version and the Version of Record. Please cite this article as doi: 10.1111/php.13118

resonance (SPR) due to the introduction of Ag NPs on the surface of the catalyst. Also, the formation of heterojunction between AgBr and mesoporous-WO_3 in Ag/AgBr@m-WO_3 significantly inhibited the recombination of light-induced electron-hole pairs in the semiconductor composite. The morphological and optical characterizations of the synthesized photocatalysts (Ag/AgBr@m-WO_3) were carried out using SEM, TEM, XDR, N_2 adsorption-desorption, UV-VIS diffuse reflectance spectroscopy (DRS). Also, the photocatalytic studies using radical scavengers were carried out and the results indicated that $O_2^{\bullet -}$ is the main reactive species.

Keywords:

Heterogeneous Photo-catalysis, Surface Plasmon Resonance, Photo-degradation, Nanocomposites, Ag/AgBr@-m-WO_3, Methylparaben

INTRODUCTION

Application of heterogeneous photocatalysis in water treatment has been increasingly popular, due to its inherent simplicity, low operational cost, mild experimental conditions (temperature and pressure) and complete mineralization of the pollutants without any residual secondary pollution. Ever since Fujishima and Honda (1) reported water splitting using TiO_2 electrode, many pure, doped and composite variants of TiO_2 have been synthesized and used for various photocatalytic and solar energy applications due to many positive attributes of TiO_2, like low cost, physical and chemical stability and high efficiency. However, one of the major constraints of TiO_2 as a photocatalyst is its wide band gap energy, that limits its activity in the UV spectral region, and hence it cannot be a good photocatalyst that can be used to harness the abundant solar radiation. Also, TiO_2 in particular shows low adsorption on the hydrophobic contaminants when used as photocatalyst for the purification of water. In addition to numerous variants of doped and composite TiO_2, many other semiconductor photocatalysts like CdS, SnO_2, WO_3, SiO_2, ZnO, Nb_2O_3, Fe_2O_3 have been used for various photocatalytic applications.

The nanostructured WO_3 has been proven to be an excellent visible-light-responsive photocatalyst due to its narrow band gap energy (between 2.4 and 2.8 eV), in addition to its stable physicochemical properties, and resistance to photo corrosions (2),(3). However, the inherent band edges of WO_3 are not compatible with the oxidation and reduction potential, that favors the chemical reactions that lead to the elimination of organic substances from water. In order to overcome this problem, and at the same time harnessing other positive attributes of WO_3, many metals loaded WO_3 like Pd/WO_3 (4), Pt/WO_3 (5),(6), and its composite forms like CuO/WO_3 (7), and $CaFe_2O_4$/WO_3 (8) were used as a photocatalyst for the degradation of organic contaminants from water.

It is well-known that due to surface plasmonic resonance (SPR) effect, the noble metal (Au and Ag) decorated semiconductor materials exhibit a significant enhancement of light absorption in the wide spectral range and this breakthrough opened up a new field of plasmonic photocatalysis (9–11). In SPR, when the incident light radiation of appropriate wavelength falls on the metal surface, the coherent oscillations of electrons in the noble metal set in, and the interaction between these electronic oscillations with the incident light promotes the light absorption due to resonance effect. Another advantage of plasmonic photocatalysis is the enhancement of the desired charge separation, promoted by the formation of Schottky junction between the metal and semiconductor and the internal electric field in the junction (12),(13). Another positive feature that can be used for photocatalysis is the mesoporosity of the material and many metal oxides semiconductors with ordered mesoporous structures have shown increased photocatalytic activity in many applications (14),(15). This is due to the increased specific surface area in the mesoporous materials and its positive effect on the creation of more active sites and the enhancement of the adsorption of reactant molecules on the semiconductor surface (16). Also, ordered mesoporous channels promote quick intraparticle molecular charge transfer, and thereby prolong the lifetime of the separated electron-hole pairs by impeding their recombination, which also further helps the improvement of photocatalytic activity (17–19). Ordered mesoporous WO_3 has been extensively used for gas sensing application, and its increased affinity with gas molecules, and also due to increased surface area, but only a few studies have been performed for photo-catalytic applications (20–23).

The enhancement of the photocatalytic activity due to the increased visible light absorption brought about by the surface plasmonic effect led to the applications of many silver/silver halide (Ag/AgX, X= Cl, Br, I) nanomaterials for the photocatalytic degradation of organic pollutants. In this line, silver bromide (AgBr) as such, is proven to be an excellent photoactive material, as it readily generates electron-hole pair when the visible radiation falls on it. The photo-generated electrons combine with interstitial silver ions to form silver atom and this makes AgBr quite unstable in its pure crystal structure (24). The following chemical equations explain the above process:

$$\mathrm{AgBr} + \mathrm{hv} \rightarrow \mathrm{AgBr}\ (\mathrm{h}^+ + \mathrm{e}^-) \qquad (1)$$

$$\mathrm{e}^- + \mathrm{Ag} \rightarrow \mathrm{Ag}_0^{\mathrm{i}}\ (\mathrm{Ag}^+\text{: interstitial silver ions}) \qquad (2)$$

$$\mathrm{AgBr} \rightarrow \mathrm{Ag} + \frac{1}{2}\,\mathrm{Br}_2 \qquad (3)$$

However, many reports have confirmed that the stability of AgBr can be improved and the consequent enhancement of photocatalytic activity can be achieved by dispersing it with certain support materials like in the form of composite materials like $Ag/AgCl/WO_3$ (25), $Ag@AgBr/Bi_2WO_6$ (26), $Ag@AgBr/g\text{-}C_3N_4$ (27), Ag–AgBr@hierarchical hollow silica spheres (Ag–AgBr@HHSS) (28), $AgBr/WO_3$ (29), $Ag/AgBr/WO_3.3H_2O$ (30), mesoporous Ag/WO_3 (31), and $Ag\text{-}WO_3/SBA\text{-}15$ (32),which were reported to have an excellent visible light photocatalytic activity for various applications. It was reported in some studies that the deposition of a trace amount of silver on the surface of AgBr@m-WO_3 has affected the photocatalytic activity of AgBr@-m-WO_3 (4, 33).

In the present work, the mesoporous WO_3 was initially synthesized by sol-gel method and it was used as a support material for AgBr to form AgBr@m-WO_3 composite and subsequently, atomic Ag was introduced in the AgBr@m-WO_3 composite by photo-reduction to produce Ag/AgBr@m-WO_3 as a final product (Fig. 1).

The Ag/AgBr@m-WO_3 (with three different Ag content) were used as photocatalysts under visible light radiation for the photocatalytic removal of methylparaben in water and this photocatalytic removal was found to be quite substantial. Parabens have been used as preservatives in personal care products, pharmaceutical, cosmetic, and food stuff for a long time, due to their ability to prevent bacterial and fungal growth. Although parabens have been extensively used in most of the personal care products, the recent studies have shown that they have some adverse health effect by disrupting the endocrine system by mimicking certain hormones in the body. Particularly, parabens mimic the activity of estrogen in the body cell, which is largely associated with breast cancer. Also, there are a few reports about the ecotoxicity of trace level of paraben in water (in ng/L to μg/L level), particularly about its adverse effects on various microorganism due to continuous discharge into the aquatic environment (4),(34). Parabens are considered as “pseudo-persistent” pollutants as a result of their continuous ejection into the water bodies and this became a cause for eco-toxicological concerns (35–37).

The motivations to use Ag/AgBr@m-WO_3 as photocatalyst for this photocatalytic degradation process are (i) the enhancement of visible absorption due to surface plasmonic effect brought about by the introduction of atomic Ag (ii) the reduction of charge recombination due to the formation of metal-semiconductor Schottky junction and also the presence of mesoporosity in WO_3 and (iii) the enhancement of active sites due to the increased surface area due mesoporosity. Morphological and optical characterizations of the synthesized Ag/AgBr@m-WO_3 were also carried out to explain the observed enhancement in the photocatalytic degradation of methylparaben in water.

EXPERIMENTAL SECTION

Synthesis of mesoporous WO_3 catalyst. A measure of 1.0 g of Pluronic P-127 (Sigma-Aldrich) was dissolved in 18 ml of ethanol by stirring for 30 minutes at room temperature and to this solution, 0.01 mol of WCl_6 (Sigma-Aldrich) was added. After vigorous stirring for 2 hours, the resulting sol solution was left to gel in an open Petri dish at 40 ^{o}C overnight in which, WCl_6 hydrolyzes and polymerizes into a tungsten oxide network. In order to remove the surfactant species, the sample was calcined at 450 ^{o}C for 6 hours in air at a rate of 2.0 ^{o}C/minute.

Synthesis of Ag/AgBr@m-WO_3. A measure of 0.25 g of m-WO_3 (prepared above) and 0.12 g of Cetyltrimethylammonium bromide (CTAB) (Sigma-Aldrich) were added into 100 ml of distilled water and after stirring the mixture for 30 minutes at room temperature, 1.0 ml of $AgNO_3$ (0.1008 M) was added and stirred for a further 20 minutes. Subsequently, the above product was irradiated using visible light from a solar simulator (150 W xenon lamp) for different duration in order to produce catalysts with different contents of Ag through the photo-reduction of Ag^+ ions in AgBr into Ag^0 nanoparticles. The catalyst was washed with distilled water, dried at 80 ^{o}C for 24 hours in the dark and finally, calcined in air at 300 ^{o}C for 3 hours to obtain the Ag/AgBr@m-WO_3 catalyst with different contents of metallic Ag^0 nanoparticles in it.

Material characterization. The phase and crystallinity of the synthesized materials were investigated by X-ray diffraction (XRD, Siemens D5005) equipped with Cu anode and variable slits. The morphology and the microstructure of the synthesized materials were studied by scanning electron microscopy (SEM), Energy dispersive spectroscopy (EDX) and high-resolution transmission electron microscopy (HR-TEM) (JEM2100F, JEOL, operated at 200 KV). The diffuse reflectance spectra (DRS) were taken using a Shimadzu (UV-2450) UV-Visible spectrophotometer, where the $BaSO_4$ fine powder was used as a standard for the baseline and the spectra were recorded in the 200 to 800 nm wavelength range. A Micromeritics Tristar 3000 system was used to measure the N_2 adsorption/desorption isotherms of the samples. Prior to the measurement, the samples were degassed for 4 h at 300 °C for the composites. The surface area was calculated using the Brunauer-Emmett-Teller (BET) equation and the pore volume was calculated from $P/P^o \sim 0.95$.

Photocatalytic degradation of methylparaben under visible light. For the study of photocatalytic degradation of methylparaben, 25 ml of 10 ppm methylparaben solution and 25 mg catalyst were taken in a beaker and the suspension was magnetically stirred for 15 min in the dark to establish the adsorption-desorption equilibrium of methylparaben at the surface of the catalyst. A sample was removed after the equilibration period and constituted time zero. The suspension was irradiated at room temperature with a broadband of light source (450 W Xe arc lamp) equipped with the UV cutoff filter to allow the wavelength of light above to 400 nm, and aliquots were removed at regular time intervals, centrifuged at 13,500 rpm for 5 minutes and the suspension was filtered with a 0.22 µm filter to remove any catalyst particles in the test solution. The concentration of methylparaben in the samples was quantified using high-performance liquid chromatography (HPLC, (Prominence Modular HPLC, Shimadzu Corporation, Japan) equipped with a photodiode array detector. A C18 column (250 x 4.6 mm, particle size 5 µm) was employed. The elution phase is the mixture of methanol/water (70:30, v/v) phase at a flow rate of 1.0 mL/min and the injection volume was 20 μL. The retention time of methylparaben under these conditions was 4.0 min. For scavenger studies, 1.0 mM of EDTA, isopropyl alcohol (IPA) and 1,4-benzoquinone (BQ) were prepared for mechanistic studies for the holes (h_{vb}^{+}), hydroxide ($^{\bullet}OH$) and superoxide radicals ($O_2^{-\bullet}$) respectively.

RESULTS AND DISCUSSION

Morphological characterization

XRD patterns of mesoporous WO_3 and the Ag/AgBr-loaded WO_3 samples are shown in Fig. 2. The XRD pattern for m-WO_3 fits with that of monoclinic WO_3 (PDF 01-072-0677). Loading with Ag/AgBr did not change the crystal structure of the support although the intensity of the WO_3 peaks decreased with higher loadings of Ag/AgBr (Figs. 2b-d). At the same time, three new peaks at 31.0^{o}, 44.2^{o}, and 72.2^{o}, appeared which can be assigned to face-centered cubic AgBr (PDF: 06-0438). However, the XRD peaks for Ag nanoparticles are not shown due to low amounts of the Ag^{o} nanoparticles and/or their small size as reported in earlier works of Ag/AgBr/TiO_2, AgBr/BiOBr and Ag/AgBr/WO_3 nanocomposites (38),(39).

High-magnification scanning electron microscopy (SEM) images were taken of m-WO_3 (Fig. 3a) and Ag/AgBr@m-WO_3 taken after 30 minutes of irradiation (Fig. 3b). The Ag/AgBr@m-WO_3 composite consists of spherical particles, whose grain size cannot be approximately estimated from the SEM. SEM images with higher resolution were not obtained as AgBr may get decomposed by the high-energy electron beam. SEM-EDX elemental mappings (Figs. 3c-f) confirm the presence of W, O, Br and Ag, respectively. On comparing Fig. 3(e) with 3(f), we can observe that the distribution of Ag is higher than that of Br. This is because Ag is present as Ag metal as well as AgBr on the surface of mesoporous WO_3. Fig. 3(f) also shows that the distribution of Ag particles is homogeneous.

The mesoporous structure of the catalyst was further studied by HR-TEM (Fig. 4). The TEM image of WO_3 shows rectangular plate-like structure (Fig. 4a) while the 30 min. Ag/AgBr@m-WO_3 shows a combination of oval and spherical shapes (Fig. 4b). The particle sizes were in the range of 10 - 50 nm. The inter-planar distances determined from the high-resolution image were found to be 0.362, 0.283 and 0.251 nm, which are consistent with the spacing of m-WO_3 (200), AgBr (200),(25),(40) and Ag (111) planes, respectively. This confirms the homogenous distribution of Ag/AgBr nanoparticles on the surface of mesoporous WO_3. The specific surface and the pore volumes of m-WO_3 and Ag/AgBr@m-WO_3 are summarized in Table 1.

Fig. 5 shows the typical deconvoluted XPS spectra of Ag and Br in 30 min Ag/AgBr@ m-WO_3, which confirms the coexistence of Ag and Br in the surface of mesoporous WO_3 surface. The peak of $Ag3d_{5/2}$ and $Ag3d_{3/2}$ appeared at 367.3 and 373.8 eV, respectively. The Ag 3d $_{3/2}$ peak resolved into 373.3 and 373.8 eV, and two peaks of 367.8 and 368.4 contributed to the peak Ag $3d_{5/2}$, respectively. According to Zhang et al (41), the peak at 373.8 and 367.8 eV were attributed to Ag^0 and the separation of 6.0 eV which also indicates the existence of metallic silver in the 30 min Ag/AgBr@m-WO_3 (42). The peak of Ag 3d which appeared at 373.3 and 367.7 eV belong to Ag^+, suggesting the existence of AgBr on the photocatalyst (43)(44).

Optical characterization

In order to eliminate the effect of light scattering by a particle in the absorption spectra, the diffuse reflectance spectra were transformed into Kubelka-Munk function (45–47). From Fig. 6, it is quite clear that as compared to pure m-WO_3, Ag/AgBr@-m-WO_3 shows enhanced absorbance, particularly in the visible region of the spectrum. Moreover, Ag/AgBr@-m-WO_3 with 30 minutes of irradiation has much stronger absorption in the visible region, compared to one with 15 minutes of irradiation. This indicates that Ag nanoparticles were effectively deposited into the photocatalyst composite and the SPR of Ag nanoparticles in Ag/AgBr@m-WO_3 is responsible for the enhancement of the visible light absorption (48). The inset in Fig. 6 shows the Tauc plots (49) for m-WO_3 and Ag/AgBr@m-WO_3. The band gap energies of the materials were determined and listed in Table 1. The band gap energy of m-WO_3 is 2.6 eV, and giving allowance for the statistical error, the change of bandgap energy due to the introduction of Ag/AgBr is not appreciable.

Photocatalytic degradation of methylparaben

The Ag/AgBr@m-WO_3 composites with different contents of atomic Ag (due to different photo- reduction time during synthesis) and pure m-WO_3 were used as photocatalysts for the degradation of methylparaben in water under visible radiation of wavelength $\lambda \geq 400$ nm. As can be seen from Fig. 7, the photocatalytic degradation of methylparaben over m-WO_3 is not appreciable compared to the Ag/AgBr@m-WO_3 composites. Ag/AgBr@m-WO_3 with the photoreduction time of 30 minutes (during synthesis) was the best performer with 85% degradation of methylparaben after 180 minutes under visible light radiation.

This result indicates that the presence of Ag/AgBr plays a significant role in the photocatalytic degradation of methylparaben.-The degradation rate of 30 min Ag/AgBr@m-WO_3 was three times faster than the m-WO_3. From the linear plots of $-\ln(C/C_o)$ vs irradiation time, it can be deduced that the photodegradation of methylparaben follows pseudo-first order kinetics (Fig. 8). The rate constants for the photodegradation can be obtained from the slopes of linear plots and are listed in Table 1. The photocatalytic degradation of methylparaben in water can be ranked in the following order: 30 min Ag/AgBr@m-WO_3 > 45 min Ag/AgBr@m-WO_3 > 15 min Ag/AgBr@m-WO_3 > m-WO_3.

In Ag/AgBr@m-WO_3 with 15 minutes of photo-reduction (during synthesis) the content of atomic silver is smaller compared to Ag/AgBr@m-WO_3 with 30 minutes of photo-reduction. Consequently, the SPR effect is reduced which leads up to less visible light absorption (Fig. 6), and weaker photocatalytic degradation of methylparaben in water. On the other hand, when the Ag content in Ag/AgBr@m-WO_3 is beyond a certain limit, as for the sample with 45 minutes of photoreduction, a portion of the Ag nanoparticles become active sites that promote the undesirable electron-hole recombination and consequently the photocatalytic activity is diminished. Also, a higher content of AgBr in m-WO_3 will lead to the formation of nanoclusters of Ag/AgBr species, which reduces the active sites on the surface of m-WO_3 through agglomeration of the particles (50),(51). The weight % of AgBr on 15 min, 30 min and 45 min of Ag/AgBr@m-WO_3 catalyst was 0.65 %, 0.81% and 1.0 % AgBr respectively. In addition to the photocatalytic activity, the stability and the reusability of Ag/AgBr@m-WO_3 were investigated (Fig. 9). The photoactivity of the catalyst remained quite stable even after five cycles of use.

The degradation rate of 30 min Ag/AgBr@m-WO_3 was three times faster than the m-WO_3. Th degradation rate follows pseudo-first order reaction which indicates that the ratio Ag and AgBr were significant parameters on the rate of photodegradation. In order to quantify the photocatalytic degradation of methylparaben in water with three different variants of Ag/AgBr@m-WO_3, we transformed the photocatalytic degradation curves in Fig. 7 in a linear form (-ln (C/C_0) vs. irradiation time) and are shown in Fig. 8. The photocatalytic degradation of methylparaben follows the pseudo-first-order kinetic model and the slopes of the above linear graphs represent the photocatalytic degradation rate constants, which are listed in Table 1 for all the catalysts used in this work. The photocatalytic degradation rate constant for methylparaben with 30 min Ag/AgBr@m-WO_3 is 0.00991 min^{-1}, which is much higher than the same with m-WO_3. In addition to the photocatalytic activity, we examined the stability and the reusability of Ag/AgBr@m-WO_3 and the results are summarized in Fig. 9, which shows that all the catalysts are quite stable even after five cycles of use with the photocatalytic reaction time of 10 minutes for each cycle. The photoactivity of the catalyst remained quite stable even after five cycles of use.

Mechanism of methylparaben degradation

Free radical and holes scavenging experiments. In order to understand the interaction between Ag/AgBr and mesoporous WO_3 and the active species generated during the photocatalyzed degradation of methylparaben using Ag/AgBr (using m-WO_3) and Ag/AgBr@m-WO_3, we carried out the holes (h_{vb}^+) scavenging and free radical experiments and the results are in Fig. 10.

In this part of the study, EDTA, isopropyl alcohol (IPA) and 1,4-benzoquinone (BQ) were used as holes (h_{vb}^{+}) scavenger, hydroxyl radical scavenger ($^{\bullet}OH$), and superoxide radical scavenger ($O_2^{\bullet -}$) (2),(3). The addition of isopropyl propyl alcohol ($^{\bullet}OH$ scavenger) did not bring about any change in the photocatalytic degradation of methylparaben, while BQ ($O_2^{\bullet -}$ scavenger) and EDTA (holes scavenger) decreased the catalytic activity (4),(5). Generally, the more the role of the reactive species, the more reduced would be the photoactivity. Hence, on this basis, our results indicate that the $^{\bullet}OH$ radical has no active role and $O_2^{\bullet -}$ was the main active species in the degradation of methylparaben. As the photodegradation was also suppressed by the addition of EDTA, it shows that holes (h_{vb}^{+}) also play a role. Knowing that the holes (h_{vb}^{+}) mostly accumulate on the valence band of AgBr and it can oxidize bromide ion to bromine atoms, which function as a reactive species to degrade methylparaben (52),(53). This explains the minor effect of the holes in the degradation of methylparaben.

Charge transfer mechanism. Fig. 11 describes the proposed charge transfer mechanism for the photodegradation of methylparaben over the Ag/AgBr@m-WO_3 composite catalyst. In Ag/AgBr@m-WO_3, the charge separation is promoted by the formation of Schottky junction between the metal and semiconductor and by the formation of a heterojunction between AgBr and mesoporous-WO_3 in Ag/AgBr@m-WO_3. These two routes of charge separation effectively reduce the photo-generated electron-hole recombination and make them available for efficient photocatalytic degradation of methylparaben. When Ag/AgBr@m-WO_3 is irradiated with visible light, photoexcited electron-hole pairs are generated in AgBr, m-WO_3, and plasmon excited Ag nanoparticles. The photo-generated electrons from Ag nanoparticles migrate to the conduction band of WO_3 and convert O_2 adsorbed on WO_3 to $O_2^{\bullet -}$. At the same time, the photo-generated holes (h_{vb}^{+}) are trapped by AgBr particles due to surface plasmon state of silver nanoparticles (54) and this mechanism results in the efficient charge separation. Another charge separation is mediated by the migration of photogenerated electron into the metallic silver on the surface of WO_3 (55) and at the same time, holes (h_{vb}^+) from AgBr oxidize Br^- to Br^0. In addition to these charge transfer mechanisms, methylparaben can directly be oxidized by the plasmon-induced h^+ (or Ag^+) on the silver nanoparticles, and this also accelerates the process of transforming photo-oxidized Ag nanoparticles back to their initial state. Mesoporous WO_3 provides more adsorption active sites for pollutant due to the higher specific surface area. The photocatalytic studies using radical scavengers were carried out and the results indicated that $O_2^{\bullet -}$ is the main reactive species. However, the role of AgBr is to mediate the spatial charge separation of photo-excited electron-hole pairs and thereby reducing the charge recombination and make more photo-generated charges available for the degradation process through the formation of $O_2^{\bullet -}$.

Major by-products of methylparaben and reaction pathways. To characterize photocatalytic by-products of this reaction, experiments were carried out at ambient conditions (1.0 mg L^{-1} of Ag/AgBr@m-WO_3 as photocatalyst) using the stock solution of methylparaben (10 mg L^{-1}) in the visible spectral region. Samples were withdrawn for analysis after 180 and 240 minutes of irradiation and were analyzed by LC-MS to identify the intermediates (Fig. 12).

In the current study, an effort was made to explain the mechanism and reaction pathways through the by-products identification, formed during the photocatalytic treatment procedure of methylparaben. Fig. 12 shows the suggested chemical formula and the value of detected ion exact mass for identified products of the degradation, during the methylparaben photocatalytic degradation process. Overall, five of the by-products was tentatively identified from the screening of the treated samples, followed by the reaction pathway of the methylparaben degradation in analyzed samples. As T. Velegraki et al (56) reported the methylparaben degradation proceed by three different ways: (i) hydroxide radical attack on the methylparaben, (ii) the reaction of methylparaben with photo-generated hole generated in WO_3 and (iii) direct oxidation of methylparaben by dissolved oxygen in water. During the treatment, the methylparaben toxicity or at least part of it remains in the solution because most of the by-products of methylparaben contain the core structure of the compound.

When the methyl group of methylparaben and hydrogen in the aromatic ring are attacked by hydroxide radical, 4-hydroxybenzoic acid **(1)** and **(2)** dihydroxybenzoic acid are produced. Also, the last product is further oxide to phenol **(3).** The formation of 1, 2-benzenedicarboxylic acid bis-(2 methylpropyl) ester **(4)** and benzendicarboxylic acid **(5)** could be attributed to coupling at high concentration (57). Furthermore, the formation of **(4)** and **(5)** could be attributed to the addition of 3-methylbutanoic acid group at the aromatic ring at C-2 and the di-hydroxylation and consequently addition of isobutene and methyl moieties at methyl acetate group, respectively.

CONCLUSIONS

In this study, highly ordered mesoporous WO_3 was synthesized by sol-gel method and subsequently, deposition-precipitation method was employed to synthesize AgBr@m-WO_3. Different levels of atomic silver were generated on the surface of AgBr@m-WO_3 by photoreduction method to get Ag@AgBr-m-WO_3. The synthesized material was used as a photocatalyst for the degradation of methylparaben in water. It was observed that the presence of Ag/AgBr on the surface of m-WO_3 brought about a significant enhancement in the photocatalytic performance of Ag/AgBr@m-WO_3 nanocomposite. The enhancement of photocatalytic degradation can be attributed to the SPR due to atomic Ag and consequent enhancement of visible absorption, the reduced of charge recombination due to the formation of metal-semiconductor Schottky junction and the enhancement of surface area due to mesoporosity. Morphological and optical characterizations of the synthesized Ag/AgBr@m-WO_3 were also carried out to explain the efficiency of this photocatalytic material in the process of removal of methylparaben in water.

Acknowledgements

We thankfully acknowledge the support of this work by KFUPM through the project # NUS15109 and NUS 15110 under the Center of Excellence for Scientific Collaboration with NUS. The support of Chemistry and Physics Departments of KFUPM is acknowledged.

References

1. Fujishima, a and Honda, K. (1972) Electrochemical photolysis of water at a semiconductor electrode. *Nature* **238**, 37–38.

2. Pan, C. and Zhu, Y. (2010) New Type of BiPO4 Oxy-acid salt photocatalyst with high photocatalytic activity on degradation of dye. *Environ. Sci. Technol.* **44**, 5570–5574.

3. Chen, C., Wang, Q., Lei, P., Song, W., Ma, W. and Zhao, J. (2006) Photodegradation of dye pollutants catalyzed by porous K3PW 12O40 under visible irradiation. *Environ. Sci. Technol.* **40**, 3965–3970.

4. Li, G., Wong, K. H., Zhang, X., Hu, C., Yu, J. C., Chan, R. C. Y. and Wong, P. K. (2009) Degradation of Acid Orange 7 using magnetic AgBr under visible light: The roles of oxidizing species. *Chemosphere* **76**, 1185–1191.

5. Cao, J., Xu, B., Luo, B., Lin, H. and Chen, S. (2011) Preparation, characterization and visible-light photocatalytic activity of AgI/AgCl/TiO2. *Appl. Surf. Sci.* **257**, 7083–7089.

6. Wang, P., Huang, B., Zhang, X., Qin, X., Jin, H., Dai, Y., Wang, Z., Wei, J., Zhan, J., Wang, S., Wang, J. and Whangbo, M. H. (2009) Highly efficient visible-light plasmonic photocatalyst Ag@AgBr. *Chem. - A Eur. J.* **15**, 1821–1824.

7. Liu, H., Cao, W., Su, Y., Wang, Y. and Wang, X. (2012) Synthesis, characterization and

photocatalytic performance of novel visible-light-induced Ag/BiOI. *Appl. Catal. B Environ.* **111–112**, 271–279.

8. Zang, Y. and Farnood, R. (2008) Photocatalytic activity of AgBr/TiO2 in water under simulated sunlight irradiation. *Appl. Catal. B Environ.* **79**, 334–340. 9. Wang, P., Huang, B., Zhang, Q., Zhang, X., Qin, X., Dai, Y., Zhan, J., Yu, J., Liu, H. and Lou, Z. (2010) Highly efficient visible light plasmonic photocatalyst Ag@Ag(Br,I). *Chem. - A Eur. J.* **16**, 10042–10047.

10. Xiao, M., Jiang, R., Wang, F., Fang, C., Wang, J. and Yu, J. C. (2013) Plasmon-enhanced chemical reactions. *J. Mater. Chem. A* **1**, 5790.

11. Wang, H., Liu, Y., Li, M., Huang, H., Xu, H. M., Hong, R. J. and Shen, H. (2010) Multifunctional TiO2 nanowires-modified nanoparticles bilayer film for 3D dye-sensitized solar cells. *Optoelectron. Adv. Mater. Rapid Commun.* **4**, 1166–1169.

12. Zhang, N., Liu, S. and Xu, Y.-J. (2012) Recent progress on metal core@semiconductor shell nanocomposites as a promising type of photocatalyst. *Nanoscale* **4**, 2227.

13. Linic, S., Christopher, P. and Ingram, D. B. (2011) Plasmonic-metal nanostructures for efficient conversion of solar to chemical energy. *Nat. Mater.* **10**, 911–921.

14. Tsung, C. K., Fan, J., Zheng, N., Shi, Q., Forman, A. J., Wang, J. and Stucky, G. D. (2008) A general route to diverse mesoporous metal oxide submicrospheres with highly crystalline frameworks. *Angew. Chemie - Int. Ed.* **47**, 8682–8686. https://doi.org/10.1002/anie.200802487.

15. Tang, J., Wu, Y., Mcfarland, W., Stucky, G. D., Lafayette, W. and May, A. (2004) Synthesis and photocatalytic properties of highly crystalline and ordered mesoporous TiO_2 thin films. 1670–1671.

16. Li, L., Krissanasaeranee, M., Pattinson, S. W., Stefik, M., Wiesner, U., Steiner, U. and Eder, D. (2010) Enhanced photocatalytic properties in well-ordered mesoporous WO_3. *Chem. Commun. (Camb).* **46**, 7620–2.

17. Chen, X. and Mao, S. S. (2007) Titanium dioxide nanomaterials: Synthesis, properties, modifications and applications. *Chem. Rev.* **107**, 2891–2959.

18. Carp, O., Huisman, C. L. and Reller, A. (2004) Photoinduced reactivity of titanium dioxide. *Prog. Solid State Chem.* **32**, 33–177.

19. Chen, X., Yu, T., Fan, X., Zhang, H., Li, Z., Ye, J. and Zou, Z. (2007) Enhanced activity of mesoporous Nb2O5 for photocatalytic hydrogen production. *Appl. Surf. Sci.* **253**, 8500–8506.

20. Qin, Y., Wang, F., Shen, W. and Hu, M. (2012) Mesoporous three-dimensional network of crystalline WO_3 nanowires for gas sensing application. *J. Alloys Compd.* **540**, 21–26.

21. Yan, X., Zong, X., Qing, G., Lu, M. and Ã, L. W. (2013) Progress in Natural Science : Materials International Ordered mesoporous tungsten oxide and titanium oxide composites and their photocatalytic degradation behavior. *Prog. Nat. Sci. Mater. Int.* **22**, 654–660.

22. Usami, Y., Hongo, T. and Yamazaki, A. (2012) Microporous and Mesoporous Materials Phosphate constituent effects on the structure and photocatalytic properties of mesoporous tungsten oxides. *Microporous Mesoporous Mater.* **158**, 13–18.

23. Yan, X., Zong, X., Lu, G. Q. (Max) and Wang, L. (2012) Ordered mesoporous tungsten oxide and titanium oxide composites and their photocatalytic degradation behavior. *Prog. Nat. Sci. Mater. Int.* **22**, 654–660.

24. Proudfoot, N. C. Handbook of photographic science and engineering.

25. Adhikari, R., Gyawali, G., Sekino, T. and Wohn Lee, S. (2013) Microwave assisted hydrothermal synthesis of Ag/AgCl/WO3 photocatalyst and its photocatalytic activity under simulated solar light. *J. Solid State Chem.* **197**, 560–565.

26. Lin, S., Liu, L., Hu, J., Liang, Y. and Cui, W. (2015) Nano Ag@AgBr surface-sensitized Bi_2WO_6 photocatalyst: Oil-in-water synthesis and enhanced photocatalytic degradation. *Appl. Surf. Sci.* **324**, 20–29.

27. Yang, Y., Guo, W., Guo, Y., Zhao, Y., Yuan, X. and Guo, Y. (2014) Fabrication of Z-scheme plasmonic photocatalyst Ag @ AgBr / g-C 3 N 4 with enhanced visible-light photocatalytic activity. *J. Hazard. Mater.* **271**, 150–159.

28. Zhang, J., Li, B. and Yang, W. (2014) One-pot synthesis of novel Ag–AgBr@HHSS with superior visible photocatalytic activity. *Microporous Mesoporous Mater.* **194**, 66–71.

29. Cao, J., Luo, B., Lin, H. and Chen, S. (2011) Photocatalytic activity of novel AgBr/WO_3 composite photocatalyst under visible light irradiation for methyl orange degradation. *J. Hazard. Mater.* **190**, 700–706.

30. Wang, P., Huang, B., Qin, X., Zhang, X., Dai, Y. and Whangbo, M. H. (2009) Ag/AgBr/WO_3-H_2O: Visible-light photocatalyst for bacteria destruction. *Inorg. Chem.* **48**, 10697–10702.

31. Sun, S., Wang, W., Zeng, S., Shang, M. and Zhang, L. (2010) Preparation of ordered mesoporous Ag/WO_3 and its highly efficient degradation of acetaldehyde under visible-light irradiation. *J. Hazard. Mater.* **178**, 427–433.

32. Gondal, M. A., Suliman, M. A., Dastageer, M. A., Chuah, G.-K., Basheer, C., Yang, D. and Suwaiyan, A. (2016) Visible Light Photocatalytic Degradation of Herbicide (Atrazine)

using Surface Plasmon Resonance Induced in Mesoporous Ag-WO3/SBA-15 Composite. *J. Mol. Catal. A Chem.* **425**, 208–216.

33. Zang, Y., Farnood, R. and Currie, J. (2009) Photocatalytic activities of AgBr/Y-zeolite in water under visible light irradiation. *Chem. Eng. Sci.* **64**, 2881–2886.

34. Gmurek, M., Bizukojć, M., Mosinger, J. and Ledakowicz, S. (2015) Application of photoactive electrospun nanofiber materials with immobilized meso-tetraphenylporphyrin for parabens photodegradation. *Catal. Today* **240**, 160–167.

35. Terasaki, M., Makino, M. and Tatarazako, N. (2009) Acute toxicity of parabens and their chlorinated by-products with Daphnia magna and Vibrio fischeri bioassays. *J. Appl. Toxicol.* **29**, 242–247.

36. Dobbins, L. L., Usenko, S., Brain, R. A. and Brooks, B. W. (2009) Probabilistic ecological hazard assessment of parabens using Daphnia magna and Pimephales promelas. *Environ. Toxicol. Chem.* **28**, 2744–53.

37. Fatta-Kassinos, D., Bester, K. and Kümmerer, K. (2013) Mass Flows, Environmental Processes, Mitigation and Treatment Strategies 'Xenobiotics in the Urban Water Cycle'.

38. Zhang, Y., Tang, Z. R., Fu, X. and Xu, Y. J. (2011) Nanocomposite of Ag-AgBr-TiO_2 as a photoactive and durable catalyst for degradation of volatile organic compounds in the gas phase. *Appl. Catal. B Environ.* **106**, 445–452.

39. Ye, L., Liu, J., Gong, C., Tian, L., Peng, T. and Zan, L. (2012) Two Different Roles of Metallic Ag on Ag /AgX / BiOX (X = Cl , Br) Visible Light Photocatalysts : Surface Plasmon Resonance and Z- Scheme Bridge. *ACS Cata.* **2**, 1677−1683.

40. Wang, P. (2016) Ag–AgBr/TiO_2/RGO nanocomposite: Synthesis, characterization, photocatalytic activity and aggregation evaluation. *J. Environ. Sci.*

41. Wang, D., Duan, Y., Luo, Q., Li, X. and Bao, L. (2011) Visible light photocatalytic activities of plasmonic Ag / AgBr particles synthesized by a double jet method. *DES* **270**, 174–180.

42. Xu, Y., Xu, H., Li, H., Xia, J., Liu, C. and Liu, L. (2011) Enhanced photocatalytic activity of new photocatalyst Ag / AgCl / ZnO. *J. Alloys Compd.* **509**, 3286–3292.

43. Yang, Y., Guo, W., Guo, Y., Zhao, Y., Yuan, X. and Guo, Y. (2014) Fabrication of Z-scheme plasmonic photocatalyst Ag@AgBr/g-C_3N_4 with enhanced visible-light photocatalytic activity. *J. Hazard. Mater.* **271**, 150–159.

44. Rong, X., Qiu, F., Zhang, C., Fu, L., Wang, Y. and Yang, D. (2015) Preparation of Ag – AgBr/TiO_2–graphene and its visible light photocatalytic activity enhancement for the degradation of polyacrylamide. **639**, 153–161.

45. Xu, H., Li, H., Wu, C., Chu, J., Yan, Y. and Shu, H. (2008) Preparation, characterization and photocatalytic activity of transition metal-loaded $BiVO_4$. *Mater. Sci. Eng. B Solid-State Mater. Adv. Technol.* **147**, 52–56.

46. Li, H., Zhang, X., Huo, Y. and Zhu, J. (2007) Supercritical Preparation of a Highly Active S-Doped TiO_2 Photocatalyst for Methylene Blue Mineralization. *Environ. Sci. Technol.* **41**, 4410–4414.

47. Wang, S. (2008) Application of Solid Ash Based Catalysts in Heterogeneous Catalysis. *Environ. Sci. Technol.* **42**, 7055–7063.

48. Wang, P., Huang, B., Dai, Y. and Whangbo, M.-H. (2012) Plasmonic photocatalysts: harvesting visible light with noble metal nanoparticles. *Phys. Chem. Chem. Phys.* **14**, 9813–9825.

49. Tauc, J. (1968) Optical properties and electronic structure of amorphous Ge and Si. *Mater. Res. Bull.* **3**, 37–46.

50. Zhu, J., Liu, S., Yang, Q., Xu, P., Ge, J. and Guo, X. (2016) Colloids and Surfaces A : Physicochemical and Engineering Aspects Fabrication of flower-like $Ag@AgCl/Bi_2WO_6$ photocatalyst and its mechanism of photocatalytic degradation. **489**, 275–281.

51. Zhuang, J., Dai, W., Tian, Q., Li, Z., Xie, L., Wang, J., Liu, P., Shi, X. and Wang, D. (2010) Photocatalytic degradation of RhB over TiO_2 bilayer films: Effect of defects and their location. *Langmuir* **26**, 9686–9694.

52. Jiang, J., Li, H. and Zhang, L. (2012) New insight into daylight photocatalysis of AgBr@Ag: Synergistic effect between semiconductor photocatalysis and plasmonic photocatalysis. *Chem. - A Eur. J.* **18**, 6360–6369.

53. Zhou, Z., Long, M., Cai, W. and Cai, J. (2012) Synthesis and photocatalytic performance of the efficient visible light photocatalyst $Ag–AgCl/BiVO_4$. *J. Mol. Catal. A Chem.* **353–354**, 22–28.

54. An, C., Peng, S. and Sun, Y. (2010) Facile synthesis of sunlight-driven AgCl: Ag plasmonic nanophotocatalyst. *Adv. Mater.* **22**, 2570–2574.

55. Hou, Y., Li, X., Zhao, Q., Quan, X. and Chen, G. (2011) TiO_2 nanotube/Ag–AgBr three-component nanojunction for efficient photoconversion. *J. Mater. Chem.* **21**, 18067.

56. Velegraki, T., Hapeshi, E. and Fatta-Kassinos, D. (2015) Solar-induced heterogeneous photocatalytic degradation of methyl-paraben. *Appl. Catal. B Environ.* **178**, 2–11.

57. Lin, Y., Ferronato, C., Deng, N., Wu, F. and Chovelon, J.-M. (2009) Photocatalytic degradation of methylparaben by TiO_2: Multivariable experimental design and mechanism. *Appl. Catal. B Environ.* **88**, 32–41.

Figure Captions:

Figure 1. Schematic for the synthesis of Ag/AgBr@m-WO_3 photocatalyst.

Figure 2. XRD patterns of (a) monoclinic m-WO_3 (b) 15 min Ag/AgBr@m-WO_3 (c) 30 min Ag/AgBr@ m-WO_3 (d) 45 min Ag/AgBr@ m-WO_3.

Figure 3. (a) High magnification SEM image of m-WO_3 particle, (b) SEM of 30 min Ag/AgBr@m-WO_3 (c) SEM-EDX elemental mapping image of W La1 on this area, (d) SEM-EDX elemental mapping image of O Ka1 on this area, (e) SEM-EDX elemental mapping image of Br Ka1 on this area and (f) SEM-EDX elemental mapping image of Ag La1 on this area.

Figure 4. TEM images of high magnification photocatalyst (a) m@WO_3 (b) 30 min Ag/AgBr@m-WO_3 (c-d) d-spacing of m-WO_3 and 30 min Ag/AgBr@WO_3 respectively.

Figure 5. XPS spectra of 30 min Ag/AgBr@ m-WO_3 (a) Ag 3d and (b) Br 3d binding energy regions

Figure 6. UV-VIS diffuse reflectance spectra represented as Kubelka-Munk Function for (a) m-WO_3 (b) 15 min Ag/AgBr@WO_3 (c) 30 min Ag/AgBr@WO_3 and (d) 45 min Ag/AgBr@WO_3 Inset shows the Tauc plots for m-WO_3 and 30 min Ag/AgBr@WO_3 in the order (a) and (c).

Figure 7. Photocatalytic degradation of methylparaben in aqueous suspension under visible light irradiation with different photocatalysts under visible light.

Figure 8. Plots of $-\ln(C/C_0)$ vs. irradiation time for the photo-catalytic degradation of methylparaben with different photocatalysts under visible light.

Figure 9. The reusability of the photo-catalyst for 30 min Ag/AgBr@m-WO_3.

Figure 10. Effect of different scavenger on the photocatalytic degradation in the presence of 30 min Ag/AgBr@m-WO_3.

Figure 11. The photo-catalytic reaction mechanism for the degradation of methylparaben.

Figure 12. Schematic for the mechanism of photocatalytic degradation of methylparaben with Ag/AgBr@m-WO_3 under visible light.

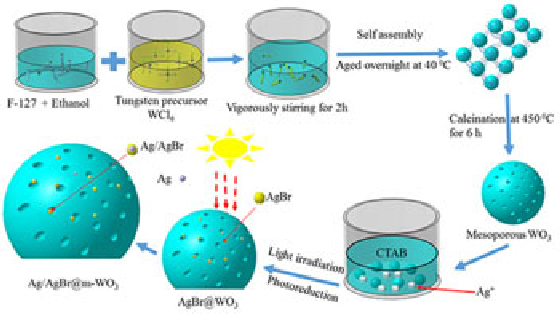
F-127 + Ethanol
Tungsten precursor WCl$_6$
Vigorously stirring for 2h
Self assembly
Aged overnight at 40 °C
Calcination at 450 °C for 6 h
Mesoporous WO$_3$
CTAB
Ag$^+$
Light irradiation
Photoreduction
AgBr
AgBr@WO$_3$
Ag
Ag/AgBr
Ag/AgBr@m-WO$_3$

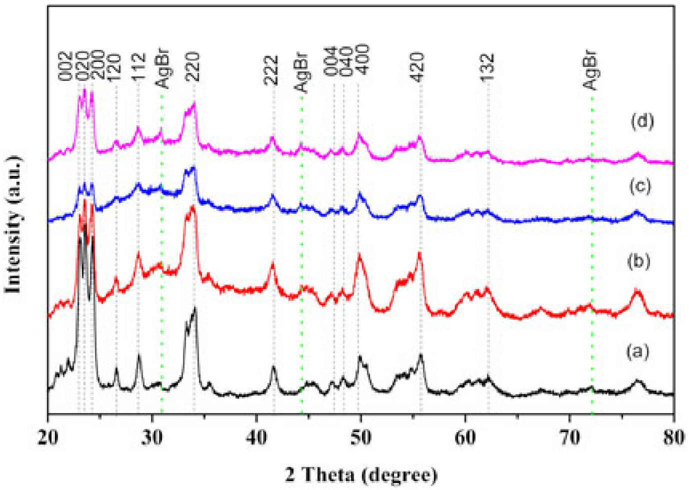
002
020
200
120
112
AgBr
220
222
AgBr
004
040
400
420
132
AgBr
(d)
(c)
(b)
(a)
Intensity (a.u.)
20
30
40
50
60
70
80
2 Theta (degree)

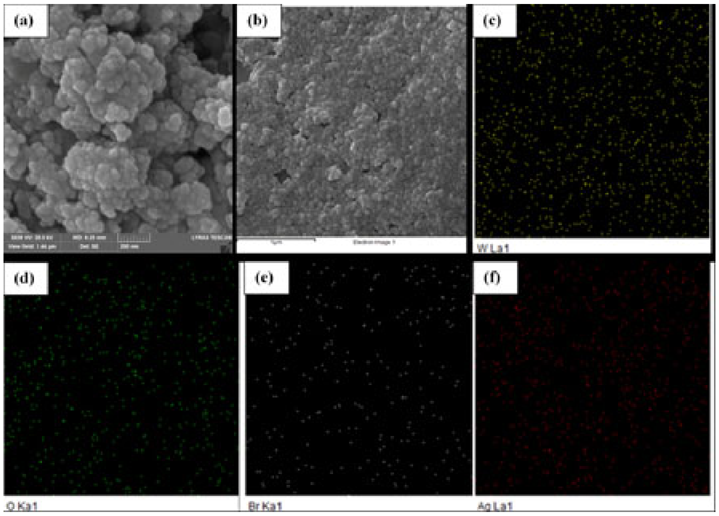
(a)
(b)
(c)
W La1
(d)
(e)
(f)
O Ka1
Br Ka1
Ag La1

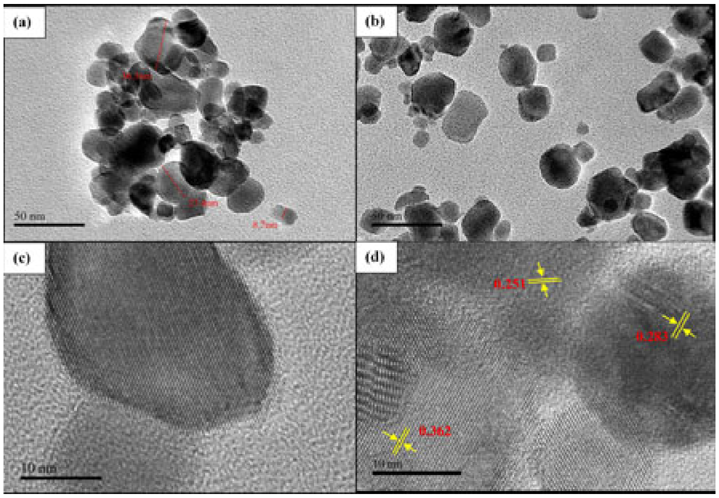
(a)
36.5nm
25 nm
8.7nm
50 nm
(b)
50 nm
(c)
10 nm
(d)
0.251
0.283
0.362
10 nm

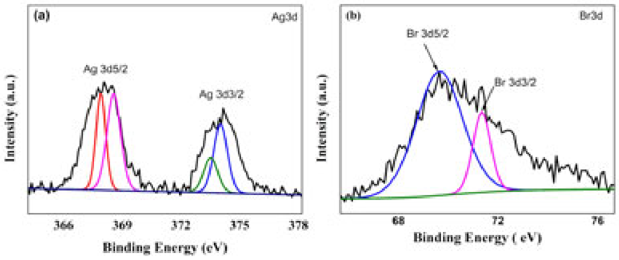
(a)
Ag3d
Ag 3d5/2
Ag 3d3/2
Intensity (a.u.)
366
369
372
375
378
Binding Energy (eV)
(b)
Br3d
Br 3d5/2
Br 3d3/2
Intensity (a.u.)
68
72
76
Binding Energy (eV)

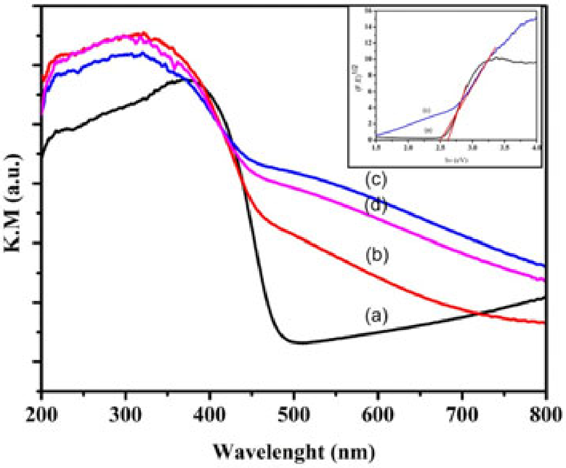
(F.E)^1/2
(c)
(a)
1.5
2.0
2.5
3.0
3.5
4.0
hν (eV)
K.M (a.u.)
(c)
(d)
(b)
(a)
200
300
400
500
600
700
800
Wavelenght (nm)

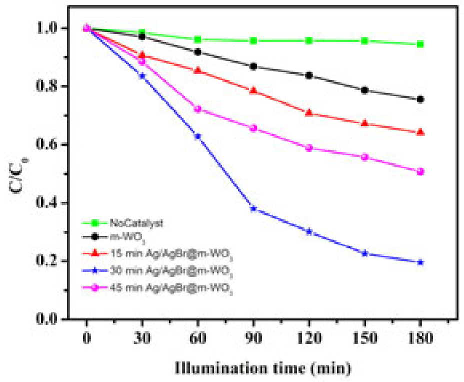
C/C$_0$
1.0
0.8
0.6
0.4
0.2
0.0
0
30
60
90
120
150
180
Illumination time (min)
NoCatalyst
m-WO$_3$
15 min Ag/AgBr@m-WO$_3$
30 min Ag/AgBr@m-WO$_3$
45 min Ag/AgBr@m-WO$_3$

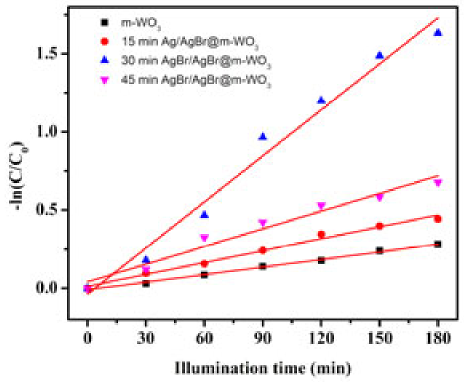
-ln(C/C$_0$)
1.5
1.0
0.5
0.0
0
30
60
90
120
150
180
Illumination time (min)
m-WO$_3$
15 min Ag/AgBr@m-WO$_3$
30 min AgBr/AgBr@m-WO$_3$
45 min AgBr/AgBr@m-WO$_3$

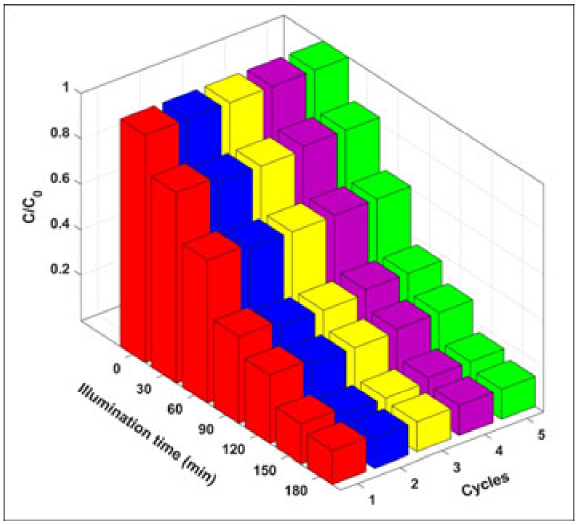
C/C$_0$
1
0.8
0.6
0.4
0.2
0
30
60
90
120
150
180
Illumination time (min)
1
2
3
4
5
Cycles

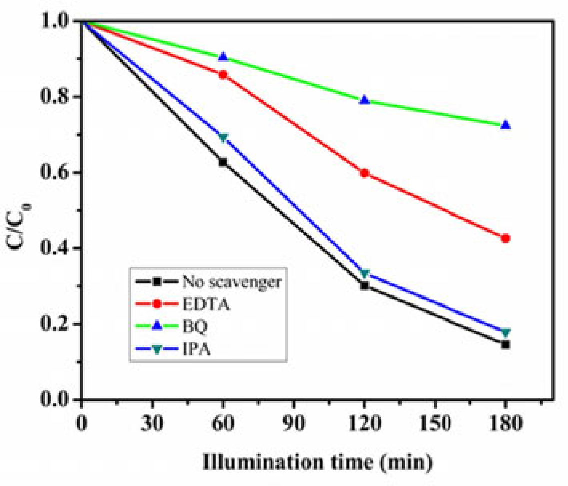
1.0
0.8
0.6
0.4
0.2
0.0
C/C$_0$
0
30
60
90
120
150
180
Illumination time (min)
No scavenger
EDTA
BQ
IPA

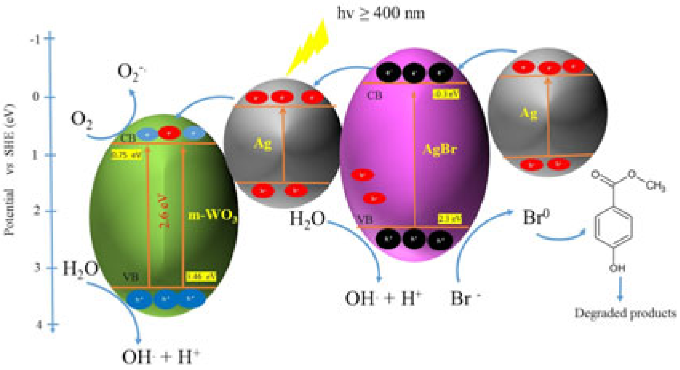
hv ≥ 400 nm
Potential vs SHE (eV)
-1
0
1
2
3
4
O$_2^{-\cdot}$
O$_2$
CB
0.75 eV
2.6 eV
m-WO$_3$
VB
3.46 eV
H$_2$O
OH$^\cdot$ + H$^+$
Ag
H$_2$O
OH$^\cdot$ + H$^+$
CB
-0.3 eV
AgBr
VB
2.3 eV
Br^0
Br$^-$
Ag
CH$_3$
OH
Degraded products

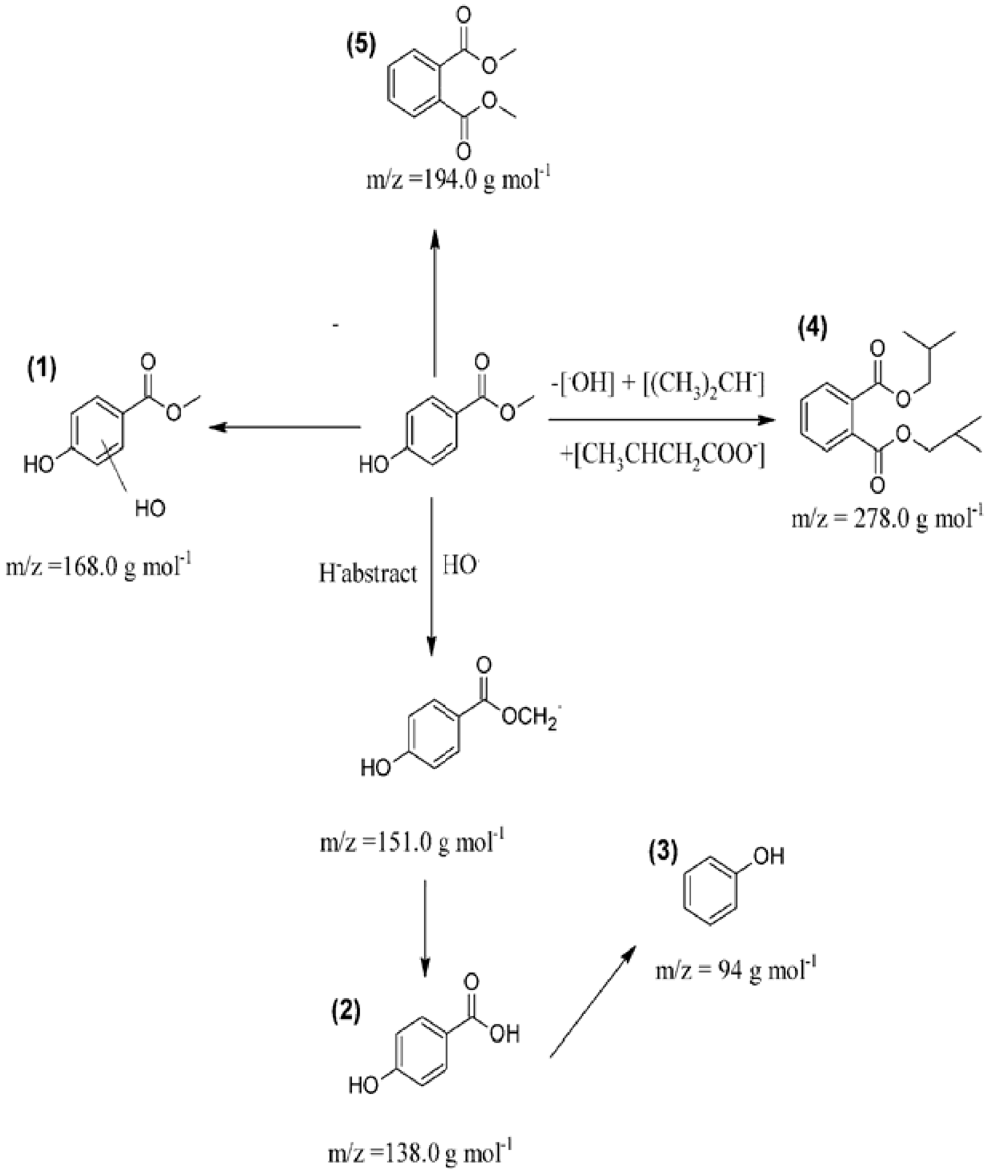
(5)
m/z =194.0 g mol-1
(1)
HO
HO
m/z =168.0 g mol-1
HO
-[·OH] + [(CH3)2CH·]
+[CH3CHCH2COO·]
(4)
m/z = 278.0 g mol-1
H·abstract
HO·
HO
OCH2·
m/z =151.0 g mol-1
(3)
OH
m/z = 94 g mol-1
(2)
OH
HO
m/z =138.0 g mol-1